4

Characterization of Carbon from the Stick of *P. juliflora* by Conventional Heating Method

4.1. Introduction

Supercapacitors are high power energy storage devices based on the fast accumulation or release of charges at the electrode electrolyte interface through electrostatic or electrochemical ion adsorption **(Yin et al., 2020)**. The high cost of porous carbon electrode active material, \$30-\$50 kg^{-1} (depending on the specific surface area and pore volumes which are the deciding factors of the capacitances of the supercapacitor) limits the popularization of supercapacitors in spite of longer cyclability, high power density, volumetric stability, large surface area, porous nature and most importantly low cost-earth abundant. An indispensable criteria with porous carbons are ultra-small electrical resistance and ultrahigh surface areas are preferred **(Liu, 2020).** The controversial believes on pore size dependence on capacitance, such as micropores are mainly responsible for high surface area and ion storage and mesopores and macropores contribute less to capacitance, with the theoretical analyses of them breaking these concepts kindle researchers to still explore carbon based electrodes endlessly **(Liu, 2020).** In addition, the unparalleled environmental issues and difficulties in the processing namely (i) Physical activation process suffers from environmental safety issues kinetics dependence and temperature problems (ii) physiochemical process have difficulty in removal of chemical agent and consequent pore clogging (iii) conventional and chemical activation process demands high cost of heating in large scale production of activated carbon.

The present work focusses on preparing porous carbon from *Prosopis juliflora* through an environmental friendly and low cost process with feasibility of large scale production. The carbon is prepared from the stick of *Prosopis juliflora*, is named as **S-Carbon** hereafter in the deliberations, through conventional heating method without any post activation process.

4.2. X-Ray Diffraction analysis of S-Carbon

The preliminary structural information of S-carbon has been analyzed by XRD analysis and the result is shown in Figure 9. The relevant XRD peaks are fitted by using Gaussian function in origin software. After fitting, the observed diffraction pattern of the S-Carbon consists prominent sharp peak at 25.23° indicating the high crystalline/ long-range ordered distribution of graphitic layers and low intense peak at 44.28° ascribed to the short-range ordered distribution of graphitic layers across the sample. The observed diffraction peaks are indexed with (002) and (101) **(Shrestha & Rajbhandari, 2021)**. Apart from these two planes, no additional peaks can be seen in the XRD pattern. Especially, the higher intensity of (002) plane indicates high degree of crystallization/ graphitization nature of the sample and is consistence with similar works published on the various biomass such as pine cone and chlorella derived activated carbon **(Bhat et al., 2019; Han et al., 2019).**

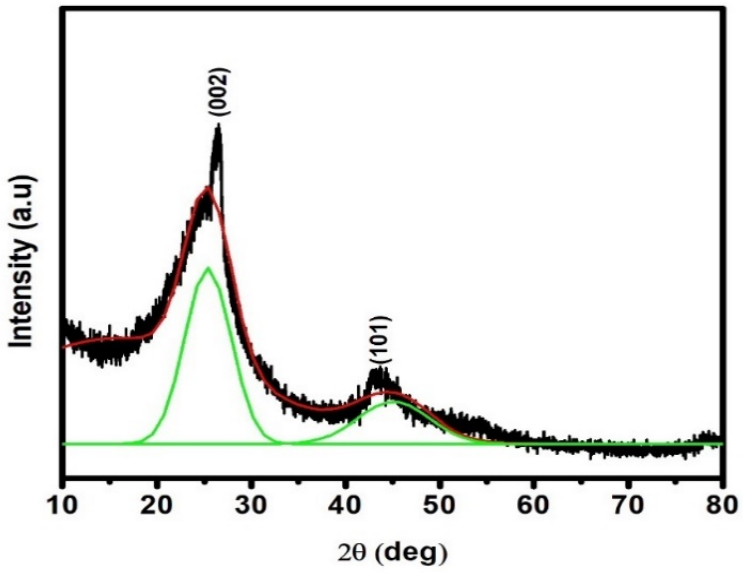

Figure 9 - X-ray Diffractogram of S-Carbon

The intensity ratio of (002) and (101) planes are compared with similar published earlier reports of such porous carbon for better understanding. The ratio is 3.25 for S-Carbon which is higher than the reported carbon from various biomasses and are listed in Table 7. The strong peak of (002) indicates the formation of graphite and high intense peak conveys the higher degree of graphitisation as well. Hence, the present attempt is a

simple, yet highly effective one for preparing graphitic carbon from biomass without any exceptional procedures/ set-ups. Further investigation on the graphitization is pursued with Raman analysis as the results are given in the following section.

4.3. Raman Analysis of S-Carbon

Raman analysis provides the structural information of prepared sample. For a clear view, the Raman spectra is fitted with Gaussian function and corresponding fit are also given in Figure 10. Generally for graphite two peaks are expected and the same are observed for S-Carbon at 1323 cm^{-1} (D band) and 1592 cm^{-1} (G band) (**Zhaojin Li et al., 2021b)** confirming the formation of graphite**.** The D band arises due to the vibration of A_{1g} mode whereas G band is due to the vibration of E_{2g} mode which relates to the sp^2 hybridization in the sample **(Zhiqian Li et al., 2021)** shown in Figure 11. The ratio of the intensity between D band and the G band (I_D/I_G) reveals the degree of graphitization / degree of the disorder **(Lazzarini et al., 2016)** of carbon prepared from the stick of *P. juliflora* material. In the present case, the intensity of the G band is higher than the D band and the ratio of I_D/I_G is 0.97 indicating high crystalline nature of the S-Carbon along with low defect distribution. A cumulative comparison of this ratio is made from the available reports on bio derived carbon for a clear understanding of the present result, Table 7. The results indicate better graphitisation in the present research work compared to other works listed in the Table 7 and the Raman spectra findings go in line with the XRD results of S-Carbon.

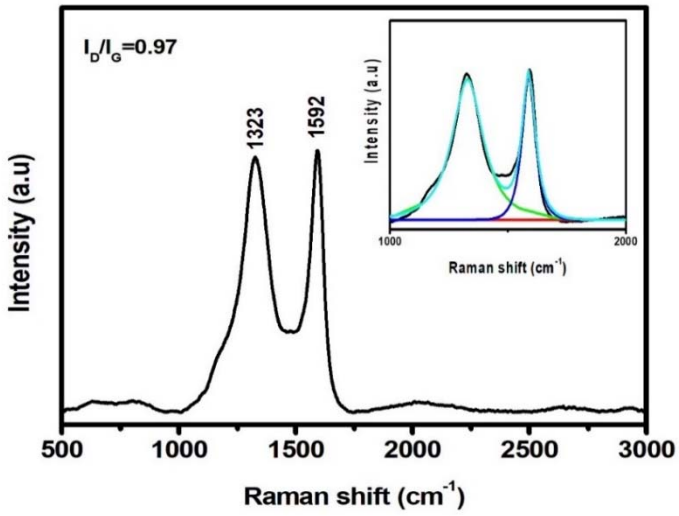

Figure 10 - Raman spectra of S-Carbon

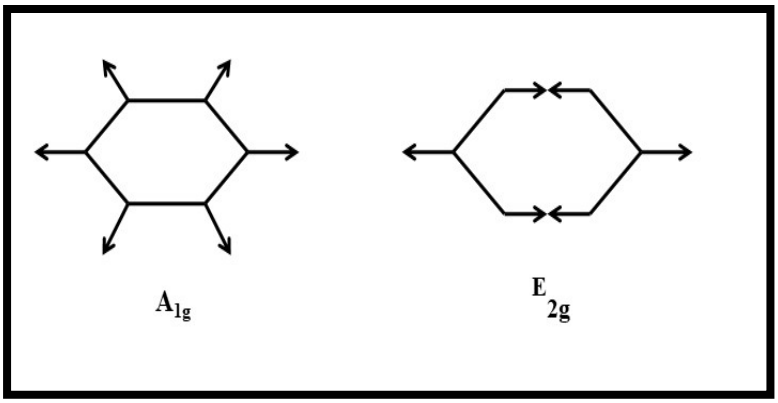

Figure 11 - A_{1g} and E_{2g} vibrational modes of the six-membered rings of the two-dimensional graphite plane

Table 7 - Comparison of XRD and Raman results of the S-Carbon with various literature

Biomass	**Method**	**Intensity ratio of (002) to (101) peak in XRD**	**I_D/I_G ratio in Raman**	**References**
Palm flower	Activation followed by hydrothermal method, centrifugation, conventional heat treatment under N_2 atm.	2.35	1.35	**Sahoo & Rao, (2021)**
Baobab	Carbonization, activation followed by heat treatment under Ar atm.	3	1.09	**Mohammed et al., (2019)**
Pecan nutshell	Activation, solar pyrolysis under Ar atm.	2.87	1.53	**Martínez-Casillas et al., (2019)**
Sweet lime peel	Activation, centrifugation and conventional heat treatment	2.1	1.18	**Ahirrao et al., (2019)**
Elm flower	Carbonization by hydrothermal method, activation followed by heat treatment under Ar atm.	1.1	1.17	**(Chen et al., (2018)**
Stick of *P.juliflora*	**Pre-activation followed by heat treatment without inert atm.**	**3.25**	**0.97**	**This work**

Larger D band is an indication of increased number of graphene layers. There is also a 2D band very feable and observed at 2691 cm^{-1}. The 2D band is an indicator of exfoliated graphene. Since it is very weak in this case, the graphite formation is confirmed but they are not cluttered to offer high peak intensity. From this result, the graphitic microcrystallite are expected to be seen in a morphological analysis. In addition, the 2D peak position can also indicate the type of conductivity can be estimated. Pristine graphene can have this peak position from 2690 to 2700 cm^{-1} corresponding to n type to p type with the wavenumber increment. In this case, the peak position is 2691 cm^{-1} which means it may be n type which may offer good conductivity in the electrochemical performance **(Das et al., 2018)**. It is not possible to compare this aspect with the listed references in the table due to non-availability of the spectral range in the articles.

4.4. FESEM Analysis of S-Carbon

The FESEM micrographs of S-Carbon at different magnifications are given in Figure 12a and 12b. The pore distribution is highly smooth in the present case as seen from the FESEM images which may be due to the ultrafine size of the graphitic carbon. Still, pores or voids like patterns are scattered throughout the sample as seen in image magnified to x 15000 at 2 μm scale. Further magnified image of this pore or void with a shorter scaling of 500 nm measures the diameter of this specific pore/void as 1.802 μm. As per the IUPAC definition, the pores are classified into three types based on their diameter. They are micro (>2 nm) /meso (2-50 nm) / macro pores (< 50 nm) respectively. Hence, the pores observed in the range of 1.802 μm can be termed as macropores of carbon sample. Further investigation of porous nature of the S-Carbon, it is highly necessary to analyze the sample by advanced studies such as HRTEM and surface area analysis such as BET.

Comparing S-Carbon with other published reports on bio-mass derived carbon materials, in same scale range of 500 nm, shows uniform distribution of pores throughout the sample which is not the case in this work **(Fasakin et al., 2018; Sahoo & Rao, 2021; Shanmugapriya et al., 2019; Xu et al., 2018)** Fasakin et al., Shanmugapriya et al. and Xu et al., have prepared the carbon from banana peel, pods of *P. juliflora* and natural casings respectively. The preparation procedure involved pre-carbonization, post-activation, carbonization and acid washing. Whereas, Sahoo and Rao have synthesized carbon from

palm flowers using KOH activation, pre-carbonization, carbonization and acid washing process. But, in the present work, carbon is prepared from the stick of *P.juliflora* biomass has been achieved exempting post activation, pre-carbonization and acid washing in the process, thereby decreasing the cost of the preparation and reduction of chemical involved in the process.

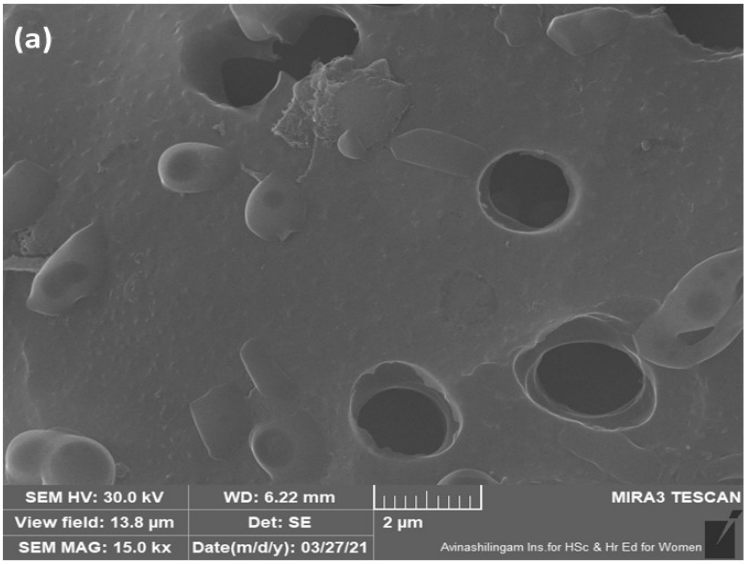

Figure 12a - FESEM micrograph of S-Carbon at lower magnification

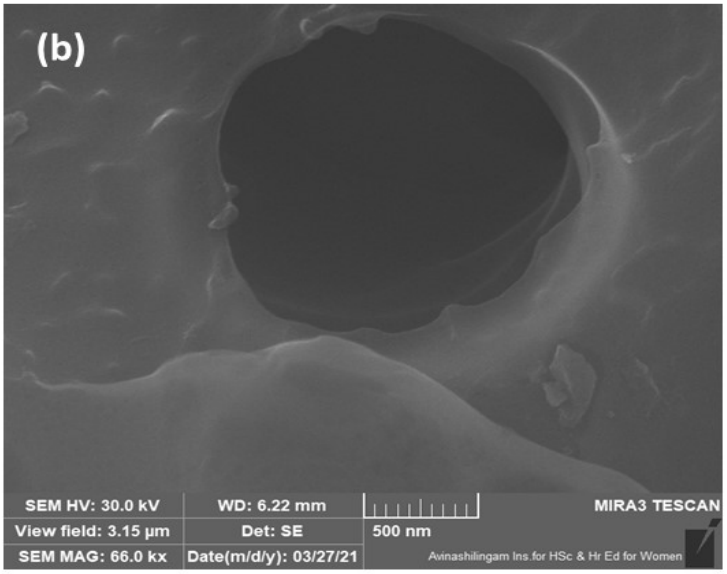

Figure 12b - FESEM micrograph of S-Carbon at higher magnification

4.5. HR-TEM Analysis of S-Carbon

HRTEM analysis clarifies further morphological aspects of S-Carbon as shown in Figure 13a and 13b. The porous nature of the S-Carbon is clearly seen in the magnified image of 50 nm scale. Apart from the pores, S-Carbon shows graphitic layers of carbon in Figure 13b which can be called as "graphitic microcrystallites". It suggests that the sample has high crystalline nature/long-range ordering of carbon. This confirms the crystallinity observed in XRD analysis and graphitization observed with Raman analysis of S-Carbon. Besides, poorly aligned spots are also seen in Figure 13b, it may be due to the effect of short range ordering of carbon across the sample. HRTEM analysis confirmed that both crystalline and short range ordered carbon has resulted from stick of *P. juliflora*. Such a mixed crystalline and short-range ordered carbon is beneficial for electrode materials to accommodate volume related issues during the charge-discharge processes for larger number of cycles. The HRTEM image is fast Fourier transformed after Z projection for better visibility of graphitic formation and disorderliness in the prepared carbon as shown in Figure 13c. Microcrystallites of graphite with ordered planes parallel to each other is clearly visible in the ImageJ processed micrograph.

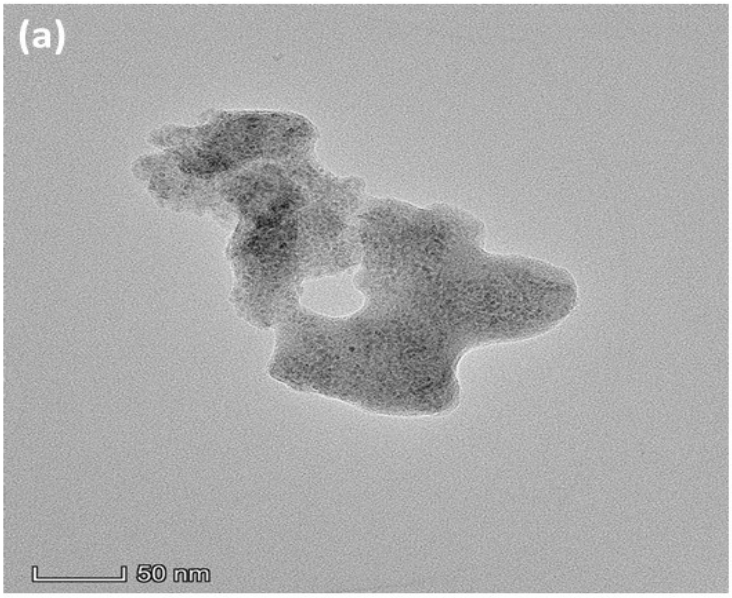

Figure 13a - HRTEM images of S-carbon at lower magnification

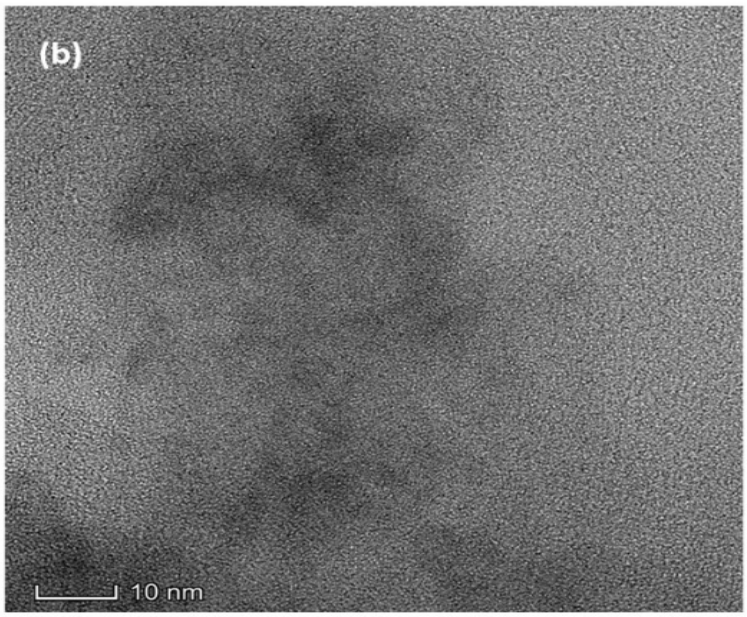

Figure 13b - HRTEM images of S-carbon at higher magnification

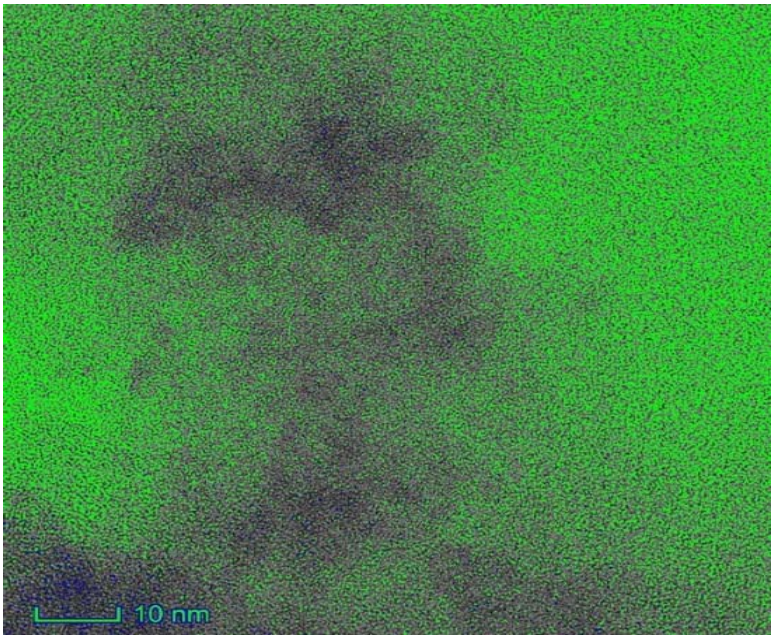

Figure 13c - FFT processed HRTEM image of S-carbon at higher magnification

4.6. Elemental Analysis of S-Carbon

The EDX analysis is carried out for estimating the elemental compositions of S-Carbon and the result is shown in Figure 14. It confirms that the prepared sample consists of significant amount of carbon along with traces of other non-cationic elements such as

oxygen (O), nitrogen (N), phosphorous (P) and metal elements such as silicon (Si), calcium (Ca) and potassium (K). The atomic weight percentages of elements in the S-Carbon are given in Table 8. Exclusively, carbon is the major component of 69.11 % whereas other elements mentioned above also co-exist with varied percentages that are present due to the existence of them in the parental *P. juliflora stick.*

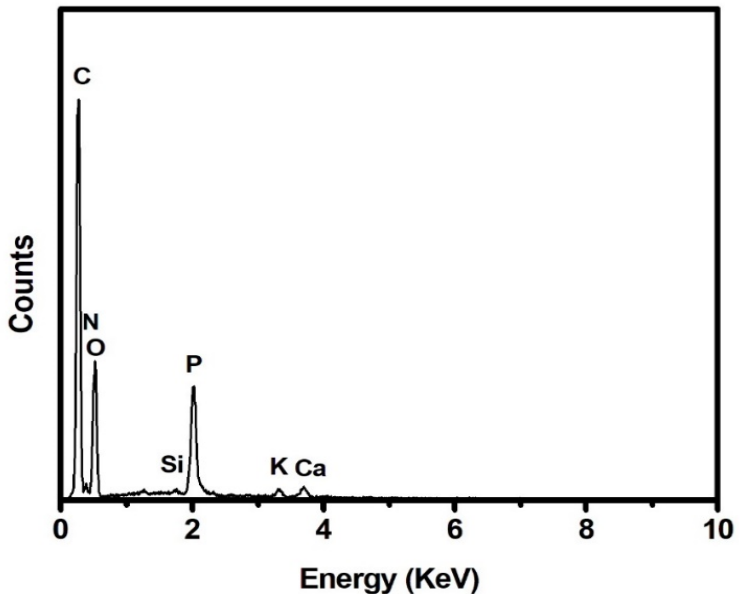

Figure 14 - EDX spectrum of S-Carbon

Table 8 - Elemental composition of carbon from the stick of *P. juliflora*

Elements	Atomic Weight %
Carbon	**69.11**
Oxygen	23.58
Nitrogen	1.32
Silicon	0.2
Phosphorous	4.63
Calcium	0.72
Potassium	0.44

Table 9 compares the atomic weight percentage of S-Carbon with the carbon prepared from various biomass resources published earlier. Comparatively, the atomic weight percentages of carbon from other resources are relatively higher than that of the present results. Still, direct comparison of present study with the other published reports cannot be a straightforward approach since the mode and steps of carbonization process has a huge difference in different cases as given in Table 9. Especially, to avoid the intervention of chemicals and to keep the preparation expenses simple, no pre-carbonization and post-chemical activation has been made in the present work. This ends up in lower weight percentage of carbon compared to the other reports. Still, the present results are more positive to successfully and effortlessly bring out effective carbon materials out of biomass resources for supercapacitor application.

Table 9 - Comparison of prepared carbon content with various literature

Biomass	**Preparation method**	**Atomic weight % of Carbon**	**References**
European deciduous tree	Pyrolysis and cavitation process	81.24	**Jain et al., (2021)**
Tissue paper	Hydrothermal reaction and activation	68.99	**Durairaj et al., (2019)**
Cucumis melo fruit peel	Carbonization, activation and heat treatment under vacuum.	83.1	**Elaiyappillai et al., (2019)**
Natural casings	Carbonization, activation and heat treatment under N_2 atm.	86.82	**Xu et al. (2018)**
Stick of *P. juliflora*	**Pre-activation and carbonization without inert atm.**	**69.11**	**Present work**

4.7. BET Surface Area Analysis of S-Carbon

The BET technique examines the porosity and specific surface area of the sample. The surface area analysis of carbon from the stick of *P. juliflora* is given in Figure 15. It shows the nitrogen adsorption at low relative pressure ($P/P_0 < 0.1$) contributed by micropores, followed by a hysteresis loop in the midrange ($0.2 < P/P_0 < 0.6$) revealing the

existence of mesopores. In addition, the rapid increase in nitrogen adsorption at high relative pressure ($P/P_0 = 0.7 – 1.0$) indicates the contribution of macropores. The surface area analysis ensured that the S-carbon consists of micro, meso and macropores throughout the sample. This is consistent with FESEM and HRTEM analysis.

The specific surface area of the S-Carbon is 6.58 m^2g^{-1} as calculated from BET analysis. This value is comparably lower than the other reports available on biomass derived carbons **(Han et al., 2018; Ojha et al., 2017; Wang et al., 2018).** Generally, the surface area of a carbon material depends on the process parameters such as biomass precursor, carbonization temperature and duration, the proportion of biomass and solvent, acid washing and so on. The prepartion procedure of S-Carbon is completely different from previously reported results which consists of predominant mircopores distribution resulting in high surface area (**Gurten Inal et al., 2018).** In the present case, due to the presence of meso and macropores the specific capacitance value has decreased. Further, presence of non-cationic and metal elements as seen in EDX spectra may clog the available pores for gas adsorption resuting in poor surface area **(Zeng et al., 2019; Zhu et al., 2018)**

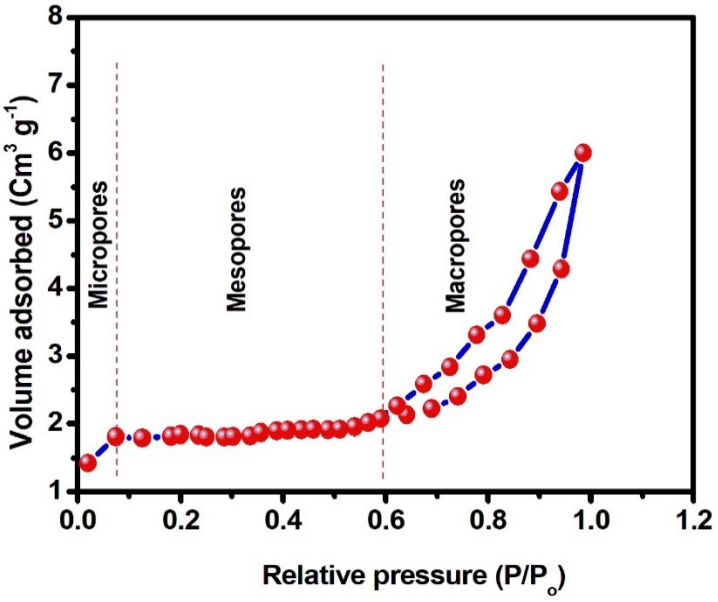

Figure 15 - BET analysis of S- Carbon

Pore volume distribution with respect to pore diameter are analyzed by Barrett, Joyner, and Halenda (BJH) method for S-Carbon. Figure 16 illustrates the distribution of pores with pore size of 3-10 nm range with deeper well having higher volume whereas

larger pores also exist but the volume of the later is lower comparatively. The moderate pore size possess moderate volume and the largest pore size > 80nm is very shallow with a lesser volume. At this juncture, it is to be kept in mind that the pore volume will have straight correspondence with charge storage in supercapacitor application. Evidently, the S-carbon has abundant mesopores and fewer macropores. These larger pores create capillary condensation during gas adsorption and creates hysteresis loop, as seen in the BET graph. Further, such a kind of larger pore distribution is the reason for possesing lower specific surface area in the sample. Narrowing the pore size distribution is one of the approaches to increase stored energy density **(Kondrat et al., 2012).** Hence, the narrowed pore size can be an advantage in this case.

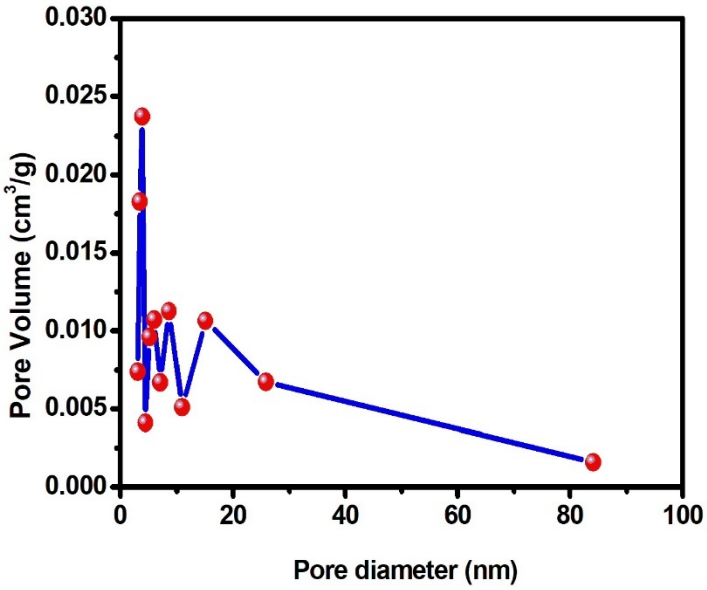

Figure 16 - Pore size distribution of S-Carbon

4.8. Electrochemical analysis of S-Carbon

4.8.1. Cyclic Voltammetry Analysis of S-Carbon

CV analysis is preferred to investigate the electrochemical behavior of S-Carbon and corresponding CV graphs at various scan rates from 10 mV/s to 100 mV/s, shown in Figure 17. The CV graph of carbon from the stick of *P. juliflora* is observed in the potential window of -0.3 V to -1.0 V, which exhibits quasi rectangular shape rather than a perfect one. Generally, a pure carbon material is expected to deliver electric double layer

capacitance (EDLC) behavior in supercapacitor applications. However, in the present case, mixed pseudocapacitive and EDLC behaviors are seen indicating the presence of two different electrochemical processes. The interpretations for such behavior are; 1) presence of non-cationic elements in the S-Carbon sample as seen in EDX analysis may supplement pseudo-capacitance **(Martínez-Casillas et al., 2019)**; 2) Surfacial reactions of non-cationic elements with the electrolyte constituents; 3) the desired behavior of Carbon electrodes' electrostatic interaction with the electrolyte solution. As a whole, the resultant pattern is observed in semi-rectangular shape rather than perfect one.

Specific capacitance can be calculated by using Eq (1) and the calculated values of S-carbon are 82, 67, 63, 59, 53 and 48 Fg^{-1} at the scan rate from 10mV/s, 20mV/s, 40mV/s, 60mV/s, 80mV/s and 100mV/s respectively. The specific capacitance value shows a decrement trend with increase in scan rate. Since the electrochemical reactions are highly surface oriented in the carbon-based anode, higher scan rate provides faster drift to the electron migration. This results in insufficient time for electron adsorption on the electrode-electrolyte interface. This results in lesser capacitance for high scan rate. However, the quasi-rectangular shape of the CV curve seen for S-Carbon is unperturbed for different scan rates which exposes the good reversibility as well as rate capability **(Omokafe et al., 2020; Wang et al., 2019).**

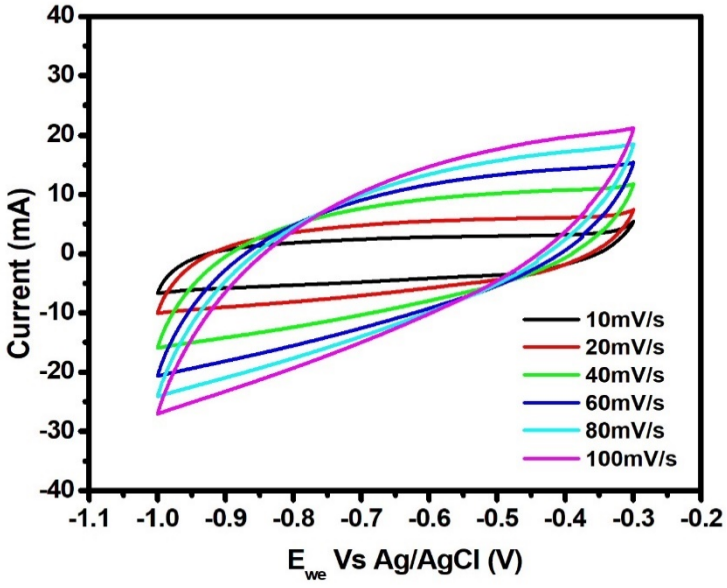

Figure 17 – Cyclic voltammogram of S-Carbon

4.8.2. Galvanostatic Charge-Discharge Analysis of S-Carbon

The capacitive behavior of S-Carbon is further confirmed by GCD analysis. In GCD analysis, stability window of the material is fixed from -1.0 to -0.3 V vs. Ag/AgCl which has been chosen from CV analysis of S-Carbon and is shown in Figure 18. Again, the GCD curves have a quasi-triangular shape which indicates that the S-Carbon contributed to the electric double layer and pseudocapacitive behavior which are very well supported by CV data **(Mohammed et al., 2019).**

The discharge curve of S-Carbon exhibits a noticeable IR drop which corresponds to the internal resistance offered by S-Carbon in the constructed electrochemical cell. The IR drop increases with the increase in current density as expected, 0.7V-1Ag^{-1}, 01V – 1.5Ag^{-1}, 0.12V – 2Ag^{-1}, 0.13V – 2.5Ag^{-1}, 0.15V – 3Ag^{-1}, not clearly seen in Figure 18. This IR drop may have arisen due to the non-cationic impurities that are observed to be present in the EDX which reduces the kinetics where lower current density allows the completion of electrochemical reaction to occur. The internal resistance, observed through IR drop, of this S-Carbon, is much smaller compared to the reported value of 0.2V **(Wei et al., 2015).**

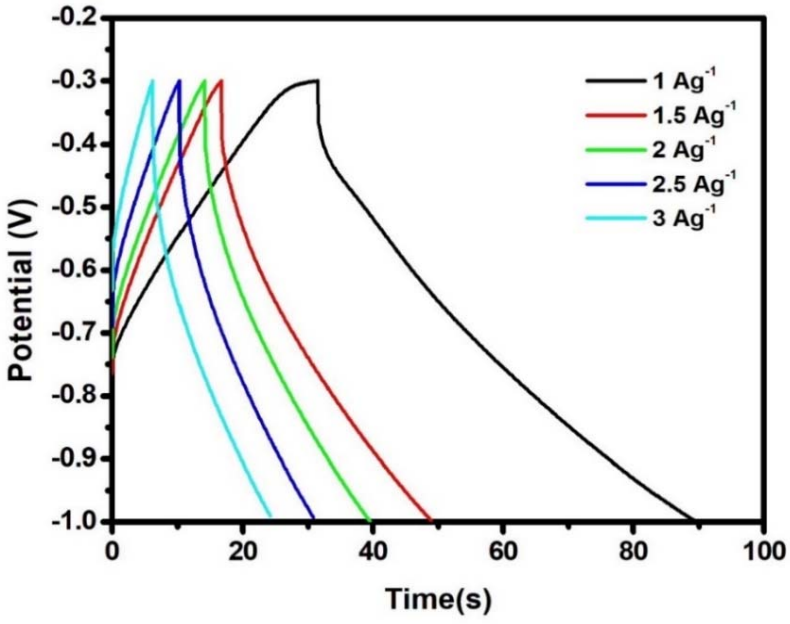

Figure 18 – Galvanostatic Charge-Discharge curves of S-Carbon

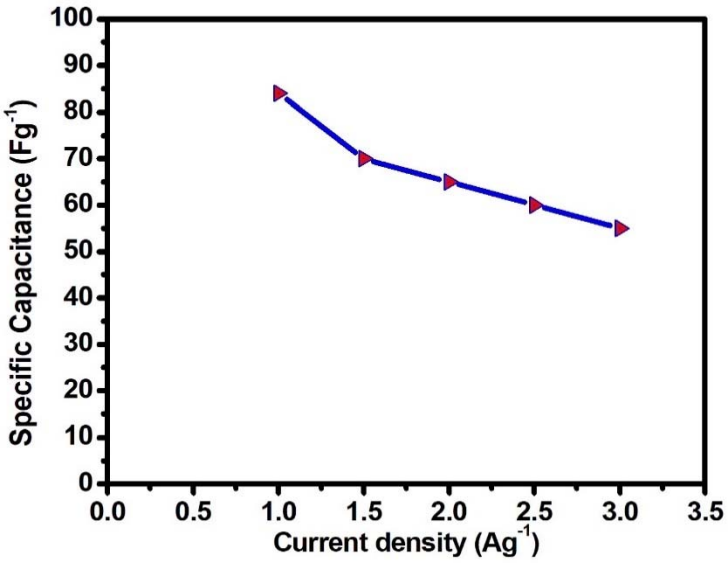

Figure 19 – Plot of current density vs specific capacitance of S-Carbon

Figure 19 shows the impact of current density on the charge-discharge process of S-Carbon material in three electrode electrochemical system. The lower current density offers more time and slower kinetics enabling the EDLC layer to persist longer thus increasing the specific capacitance. A capacitance value of 84 Fg^{-1} at 1 Ag^{-1} is observed with S-Carbon. An extensive comparison of specific capacitance and respective current density has been made on carbon materials derived from biomass resources and presented in Table 10. The current densities and specific capacitances of carbon of different biomass origin and different preparation methods are analyzed. The reports of Han et al reports only areal current density and to compare it with S-Carbon the conversion to areal current density. The reported results show 142 Fg^{-1} at 1 $mAcm^{-2}$ areal current density whereas with S-Carbon it is observed to have 84 Fg^{-1} at 3 $mAcm^{-2}$ which is superior to the Chlorella derived carbon through activation and heat treatment process with Ar atmosphere. Among the preparations made from different part of *Prosopis juliflora* by different researchers, listed in the Table 10, the present work shows second highest specific capacitance at a current density of 1 Ag^{-1} where the first one is by Shanmugapriya et al and it is to be noted that the preparation of the carbon from pods is made by hydrothermal process followed by chemical activation. Hence, a comparable performance of the S-Carbon is observed with direct cellulosic conversion of carbon in the present work.

The cyclic stability of the carbon from the stick *P. juliflora* is evaluated and shown in Figure 20. After continuous 500 charge/discharge cycles, the prepared carbon electrode material still retains 94% of its initial capacity due to the outstanding cyclic stability of the S-Carbon.

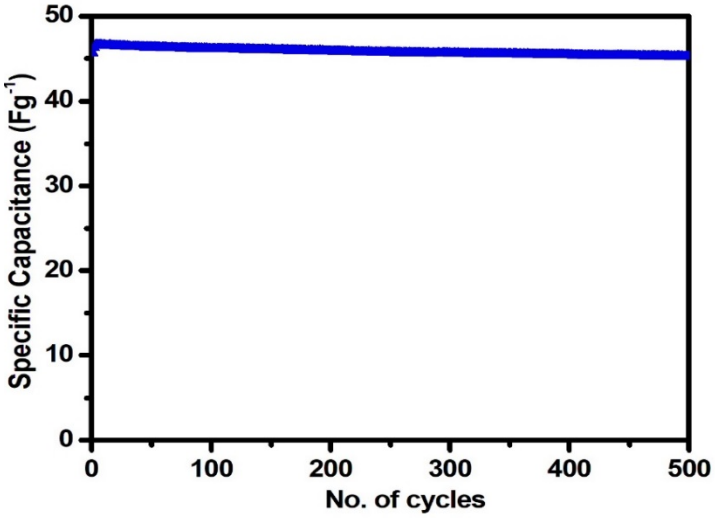

Figure 20 – Cyclic stability of S-Carbon

4.8.3. Electrochemical Impedance Analysis of S-carbon

The electrochemical impedance analysis of the electrochemical cell with S-Carbon as working electrode is measured in the frequency range of 100 mHz to 10 KHz at room temperature and the Nyquist plot is shown in Figure 21. The plot is fitted using EC lab software and corresponding equivalent circuit is given in Figure 22. The fitting parameters obtained from the equivalent circuit are shown in Table 11.

In the impedance plot, interception of the spectra on the X-axis in the high-frequency region relates to the solution resistance (R_S). It is the measure of resistance between working electrode and reference electrode. Before and after cycling, the value of solution resistance of the sample is 1.19 Ω and 1.15 Ω. The mid-frequency region of Nyquist plot has a depressed semi-circle that represents the charge transfer resistance (R_{ct}) of the material in an electrochemical system. The R_{ct} values are 4.15 Ω and 12.05 Ω before and after cycling respectively. However, the resistance value of the cell with S-Carbon before cycling is 4.15 Ω which increases to 12.05 Ω after 500 cycles. The increment in resistance of the cell is due to the solid electrolyte interface (SEI) formation on the working electrode during the process of charging and discharging.

SEI is an inactive layer coated on the working electrode material as a result of irreversible electrochemical reactions. This layer limits the effective charge migration in the electrode material which imposes some impedance towards the total internal resistance of the electrochemical cell. Followed by that, effect of diffusion is seen at the lower frequency region as a Warburg impedance in the equivalent circuit **(Kesavan et al., 2019).** The angle subtended by the low frequency spike with the horizontal origin have not changed indicating the increase in resistance does not affect the capacitive behaviour of the electrochemical cell over 500 cycles. It is also supported by the values of n1 and n2, lying from 0.87 to 0.73, indicating less diffusive behaviour of the working electrode. Also, the CPE1 and CPE2 values does not undergo much changes indicating this interpretation to be positive. Hence, the decrease in cyclic stability is purely due to the increase in internal resistance of the electrochemical cell with S-Carbon as working electrode.

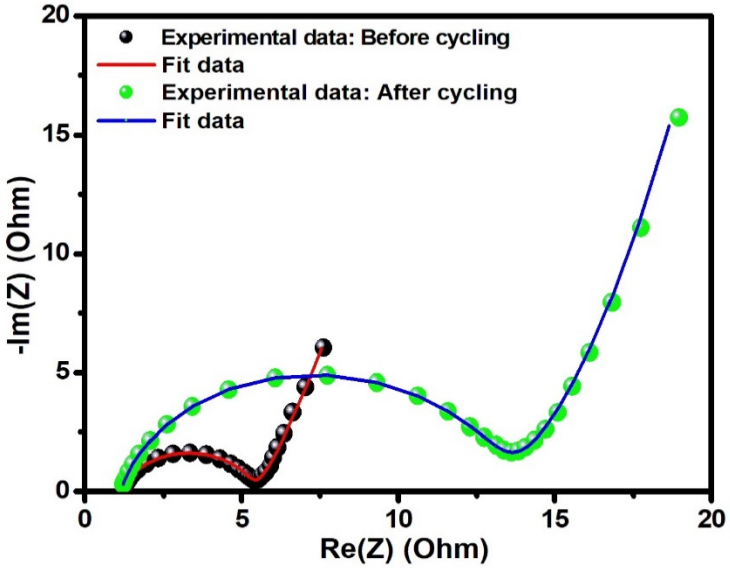

Figure 21 – Electrochemical impedance spectra of S-Carbon before and after cycling

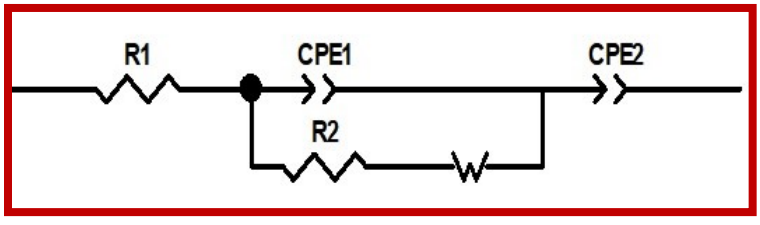

Figure 22 – Equivalent circuit obtained from electrochemical impedance spectra S-Carbon

Table 10 - Comparison of specific capacitance of prepared carbon with various literature

Material	Preparation method	Activating agent	Specific capacitance (Fg^{-1}) at Current density (Ag^{-1})	References
Wood *Prosopis juliflora*	Carbonization, activation, and heat treatment under N_2 atm.	KOH	588 @ $0.5Ag^{-1}$	**Selvaraj et al., (2021)**
Walnut shells	Activation and Pyrolysis under N_2 atm.	KOH	169.2 @ $0.5Ag^{-1}$	**Lan et al., (2020)**
Wood *Prosopis juliflora*	Activation and carbonization under N_2 atm.	KOH	198 @ $0.2Ag^{-1}$	**Selvaraj et al., (2020)**
Cassava root	Activation and carbonization	KOH	175±12 @ $2Ag^{-1}$	**Chaisit (2020)**
Pods of *Prosopis juliflora*	Hydrothermal reaction, activation, heat treatment under Ar atm.	KOH	274 @ $1.3Ag^{-1}$	**Shanmugapriya et al., (2019)**
Waste coffee grounds	Activation and carbonization under N_2 atm.	KOH	105.3 @ $0.5Ag^{-1}$	**Chiu &Lin (2019)**
Anaerobic digester residues	Carbonization, activation and Pyrolysis	KOH	184.91 @ $1Ag^{-1}$	**Wang et al., (2019)**
Chlorella	Carbonization, activation and heat treatment under Ar atm.	KOH	142 @ $1mAcm^{-2}$	**Han et al., (2019)**
Banana peel waste	Hydrothermal reaction, activation and carbonization under Ar atm.	KOH	115 @ $0.5Ag^{-1}$	**Fasakin et al., 2018)**
Loofa sponge	Carbonization, activation and heat treatment under N_2 atm	KOH	185.9 @ 0.1Ag-1	**Feng et al., (2018)**
Waste cumin plant	Activation, microwave treatment, heat treatment under N_2 atm.	H_3PO_4	155 @ 1.5 $mAcm^{-2}$	**Gurten Inal et al., (2018)**
Pineapple leaves	Carbonization, activation and heat treatment under Ar atm.	KOH	131.3 @ $5mVs^{-1}$	**Sodtipinta et al., (2017)**
Wood *Prosopis juliflora*	Carbonization, activation and heat treatment under N_2 atm.	KOH	161 @ $0.1Ag^{-1}$	**Sennu et al., (2016)**
Stick of *P. juliflora*	**Pre-treatment and carbonization with ambient atm.**	**H_2SO_4**	**84 @ $1Ag^{-1}$**	**This work**

Table 11 - Fitted parameters of electrochemical impedance spectra of S-Carbon

Parameters	S-Carbon	
	Before cycling	**After cycling**
$R_1(\Omega)$	1.19	1.15
$R_2(\Omega)$	4.15	12.05
CPE 1	0.21×10^{-3}	0.24×10^{-3}
n1	0.80	0.73
CPE 2	0.12	0.16
n2	0.87	0.82
W	1.80	4.33

4.9. Summary

Carbon is prepared using Stick of *Prosopis juliflora* (S-Carbon) by pretreatment and conventional heating method at 800°C for 2 hours. The carbon is characterized with XRD, Raman, FESEM, HRTEM, EDX, BET and Electrochemical characterization – CV, GCD and EIS for the three electrode configuration with S-Carbon as working electrode. The carbon is crystalline confirmed by XRD and Raman analysis. The I_D/I_G ratio is 0.97 indicating high graphitization. The morphological characterization indicates porous nature of the S-Carbon and long range orderliness is observed with TEM results. The micrographs are analysed with ImageJ and presented. The porosity measurement indicated mixture of micro, meso and macropores which has more relevance to the performance on capacitive contribution. The cyclability is well established for 500 cycles with higher stability of 94%. A stable capacitive contribution is also observed. The internal resistance increases with cycling due to the irreversible solid electrode-electrolyte interface formation thus incorporation of capacity fading of 6% over 500 cycles. An IR drop is observed, which is also an indicator of internal resistance, with increase in current density that leads to poor performance of S-Carbon. Hence, Bark is selected for preparation and the prepared carbon is analysed and the results are discussed in the next Chapter.